Hindawi
Geofluids
Volume 2022, Article ID 7923448, 10 pages
https://doi.org/10.1155/2022/7923448

Research Article

Experimental Study on the Evolution Mechanism of Landslide with Retaining Wall Locked Segment

Han-Dong Liu,[1] Jia-Xing Chen ,[1] Zhi-Fei Guo,[1] Dong-Dong Li,[1] and Ya-Feng Zhang[2]

[1]*College of Geosciences and Engineering, North China University of Water Resources and Electric Power, Zhengzhou 450045, China*
[2]*Zhengzhou University of Technology, Zhengzhou 450044, China*

Correspondence should be addressed to Jia-Xing Chen; b2019081814@stu.ncwu.edu.cn

Received 31 October 2021; Revised 9 December 2021; Accepted 13 December 2021; Published 11 January 2022

Academic Editor: Yi Liu

The failure of locked segment-type slopes is often affected by rainfall, earthquake, and other external loads. Rainfall scours the slope and weakens the mechanical properties of rock-soil mass. At the same time, rainfall infiltrates into cracks of slope rock mass. Under the action of in situ stress, hydraulic fracturing leads to the development and expansion of rock cracks, which increases the risk of slope instability. Under seismic force, the slope will be subjected to large horizontal inertial force, resulting in slope instability. In this paper, a self-developed loading device was used to simulate the external loads such as rainfall and earthquake, and the model tests are carried out to study the evolution mechanism of landslide with retaining wall locked segment. Three-dimensional laser scanner, microearth pressure sensors, and high-definition camera are applied for the high-precision monitoring of slope shape, deformation, and stress. Test results show that the retaining wall locked segment has an important control effect on landslide stability. The characteristics of deformation evolution and stress response of landslide with retaining wall locked segment are analyzed and studied by changing the slope shape, earth pressure, and the displacement cloud map. The evolutionary process of landslide with retaining wall locked segment is summarized. Experimental results reveal that as the landslide with retaining wall locked segment is at failure, the upper part of the landslide thrusts and slides and the retaining wall produces a locking effect; the middle part extrudes and uplifts, which is accompanied with shallow sliding; and compression-shear fracture of the locked segment leads to the landslide failure.

1. Introduction

Landslides can be divided into two types depending on whether there are locked segments that control landslide stability: locked segment type and nonlocked segment type [1]. The key to solving the problem of early warning and prediction of landslides is to study the deformation evolution and instability process of the locked segments that have a controlling role in landslides. From the perspective of the history of geological evolution, the locked segments are the "hard" rock-soil mass formed by the long-term geological evolution at the potential sliding surface. Compared to the surrounding rock and soil, the locked segments have better mechanical properties and control landslide sliding. The geological evolution of locked segments is complex and diverse. The locked segments can be "harder" boulders or rocks formed by long-term differential weathering of the slope, or "harder" intrusive rocks formed by tectonic movement or hard rocks formed by geological transport and deposition. Locked segment-type landslides are usually large and have high energy storage. Once they lose stability and slide, they often lead to high-speed and long-distance landslides with strong destructiveness. For locked segment type landslides, as long as the locked segments of the potential sliding surface do not form connected fracture surface, there is no complete failure of landslide even under the influence of rainfall, earthquake, and other external factors. Therefore, it is of great importance to study the evolution mechanism of locked segment type landslide for early landslide identification, early warning, and disaster prevention [2–6].

Methods for investigating the evolution mechanism and prediction of landslides mainly include engineering geological comprehensive analysis method, theoretical analysis method, physical model test method, and numerical

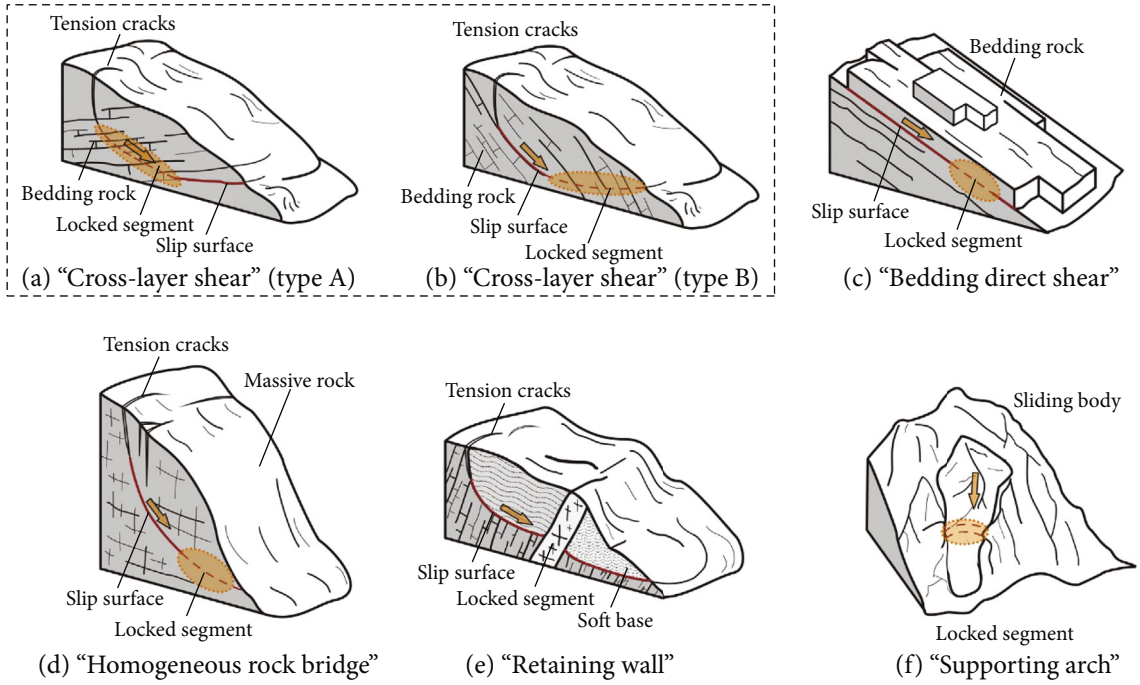

Figure 1: Classification of the locked-segment type landslides [2].

simulation method [7–13]. Many scientists have confirmed the existence of locked segments in a number of large-scale landslides [14–18]. The occurrence of large-scale landslides is generally accompanied by a sudden brittle failure of locked segments of the sliding surface [19]. According to the occurrence characteristics of locked segments, locked segment type landslides can be divided into five types: "cross-layer shear," "bedding direct shear," "homogeneous rock bridge," "retaining wall," and "supporting arch" (Figure 1) [2]. According to geological characteristics, the cross-layer shear type is further divided into two types. In a stratified slope, a potential slip surface usually intersects with the layered strata that play the role of the locked segment, such as an antidip stratified landslide (Figure 1(a)) and a dip stratified landslide whose dip angle is larger than the slope angle (Figure 1(b)) [2]. Currently, there are many researches on rock bridge-type landslide [20–25]. Different locked segment type landslides have different evolution mechanism and deformation characteristics [26, 27]. Furthermore, the landslide evolution process has complex nonlinear characteristics [4]. Based on the renormalization group theory and the locked segment concept, Qin et al. [28] proposed two universal exponential laws for the critical displacement evolution of landslides and avalanches. The same study found that the critical instability displacement of slopes depended on displacement at the onset point of accelerating creep and the number of locked segments. The Weibull distribution was used to represent the probability of block failure in the locked segment under shear condition. The behavior of brittle failure of rock was studied based on theoretical analysis. The brittle failure of rock is mainly caused by the initiation and propagation of cracks [29, 30]. The parameter m of the Weibull distribution can not only characterize the heterogeneity of rocks but also reflect the characteristics of the mechanical response of rocks under the influence of external factors, which can be used as an index to measure the degree of brittle failure of rock [31, 32]. According to the Weibull distribution and renormalization group theory, a damage constitutive model of locked segment has been established. The creep process of locked segment type landslide is divided into three stages: primary creep, secondary creep, and tertiary creep. The volume expansion point indicates that the slope enters the tertiary creep stage [33]. Taking the slope sliding displacement as the main parameter, the relationship of the shear displacement along the sliding surface at the volume expansion point, peak strength point, and residual strength point was established, and a physical prediction model of slope instability was constructed [1, 34]. Rainfall and earthquake are important external factors that induce landslides [35–45]. For rocky slopes, rainfall infiltrates into rock mass cracks. Under the long-term action of in situ stress, the water pressure in the rock mass cracks leads to further development and expansion of the cracks, which reduces the stability of the slope. Many scholars have studied the influencing factors [46, 47] and calculation models [48–50] of rock hydraulic fracture propagation through hydraulic fracturing physical model test and numerical simulation. Based on the history of geological evolution, geological environmental conditions, and engineering geological characteristics of western Henan Province in China, Liu et al. [15] proposed that the locked segment type landslides in western Henan mainly included "bedding direct shear type," "cross-layer shear type," and "retaining wall type." In the same study, they selected the Huaipa landslide, the Fengmaisi landslide, and the Dongmiaojia landslide as a typical locked segment type landslide. Based on that, the large-scale physical models of different locked segment type landslides were tested under rainfall

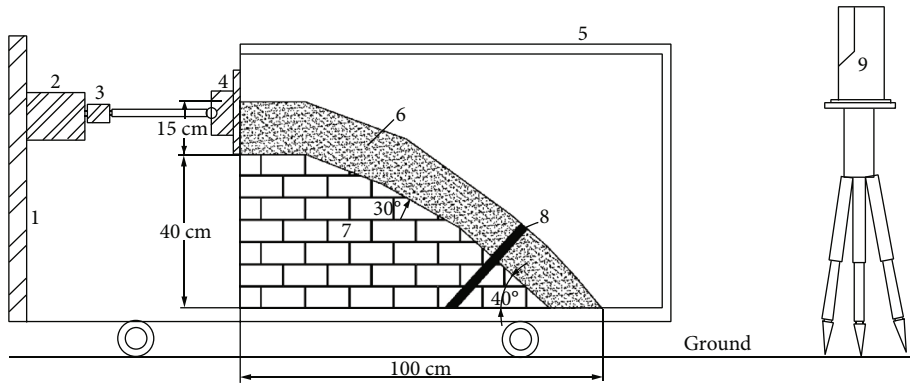

Figure 2: The experimental equipment.

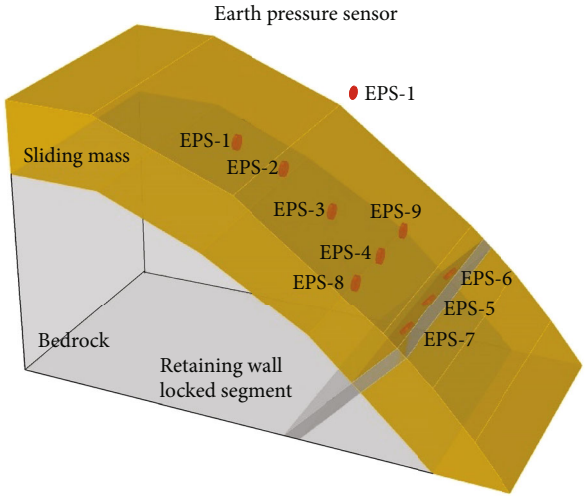

Figure 3: Locations of the earth pressure sensors (EPS).

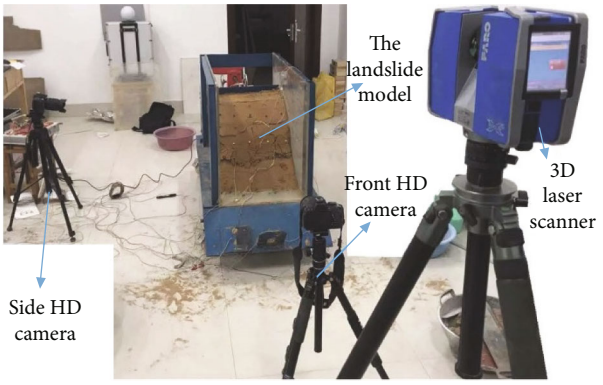

Figure 4: Landslide model and instruments layout.

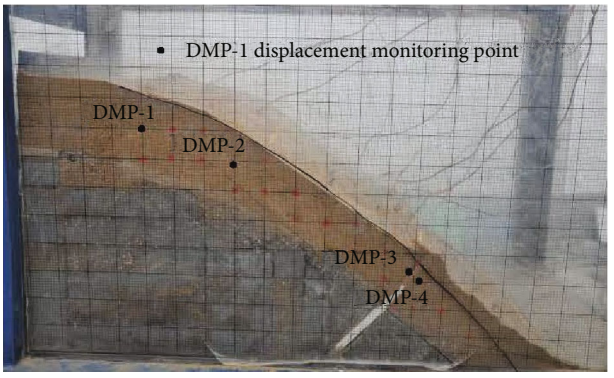

Figure 5: Displacement monitoring points on landslide side.

conditions. The catastrophe process and the macroscopic deformation instability characteristics of different types of locked segment type landslides under rainfall conditions were revealed, and the failure mechanism of locked segment type landslides caused by rainfall was expounded [51].

At present, a number of theoretical studies and physical model tests on the locked segment type landslides have been conducted, and many results of scientific research have been achieved. However, there are few studies on the failure mechanism of landslide with retaining wall locked segment. Based on a generalized geological model of the landslide with retaining wall locked segment, this paper designed a self-developed physical model testing device to investigate the failure mechanism of landslide with retaining wall locked segment. The evolution process and deformation characteristics of landslide with retaining wall locked segment are analyzed, and the failure mechanism of landslide with retaining wall locked segment is further revealed. This kind of research is of great importance for early identification, disaster warning, and landslide prevention.

2. Materials and Methods

2.1. Experimental Design. In this paper, a series of physical model tests are performed to study the failure mechanism of landslide with retaining wall locked segment. The physical model test device includes a loading system and a model box, as shown in Figure 2. The loading system is connected to the DHS 3816 acquisition instrument via a pressure sensor for load measurements. The size of the model box is

Table 1: Model tests soil mass grain content percentage.

Grain size (mm)	<0.075	0.075–0.1	0.1–0.25	0.25–0.5	0.5–1	1–2	2–5
Percentage (%)	0.41	0.49	19.23	78.10	0.93	0.28	0.56

1.15 m × 0.5 m × 0.8 m (length × width × height). The model test is mainly to study the evolutionary instability process of landslide with retaining wall locked segment. On the basis of making full use of the model box space, the size of the landslide model is set to 1.0 m × 0.5 m × 0.57 m (length × width × height), and the thickness of the sliding mass is 15 cm.

The model test used microearth pressure sensors to measure the change of earth pressure in model. The earth pressure sensor (DMTY type) is 22 mm in diameter, 6.5 mm thick, with measuring range 0-20 kPa, and full scale (FS) precision less than 0.5%. During the test, earth pressure inside the slope was recorded using DHS 3816 with the acquisition frequency of 1 Hz. In the model test, five earth pressure sensors were placed at the central axis of the landslide and located on the trailing edge, middle part, and the retaining wall of the model landslide. Four earth pressure sensors are installed on both sides of the landslide (Figure 3). Prior to the installation of these sensors, they were calibrated to ensure their sensitivity and accuracy.

The 3D laser scanner FARO X330 was used to measure the change of the slope shape during the landslide evolution and instability. The scanning accuracy is ±1 mm. During the test, the slope surface was scanned under each load, and the slope shape at different stages was recorded by three-dimensional point cloud data. Then, the three-dimensional digital terrain models of slope shape at different stages are constructed in Surfer (Golden Software, Golden, CO, USA). The deformation characteristics of the slope surface during the evolutionary instability of a landslide with retaining wall locked segment were studied by the three-dimensional terrain models at different stages. In order to reveal the formation and evolution of landslide cracks, a high-definition camera was used to take regular photographs of the slope surface (Figure 4).

In order to further monitor changes in displacement within the landslide model during the test, monitoring points were set at different positions on the side of the landslide model (Figure 5), and the high-definition camera was used to photograph the side of the landslide at different times (Figure 4). The photos taken at different times were calibrated, and the evolution process of deep displacement was studied by changing the coordinates of the monitoring points at different times.

The landslide model was loaded through the self-developed physical model test loading device (Figure 2). A total of 11 loads were performed, with an average load of 200 N/s each time.

2.2. Experimental Materials. The landslide model mainly includes sliding mass and retaining wall locked segment. Sandy soil was used as the sliding mass in order to facilitate the observation of the evolution and instability process of landslide. The grain size of the soil mass will affect its physical and mechanical properties and the process of landslide deformation. Therefore, sand sample was dried and sieved, and the percentage of different grain sizes (Table 1) and grain analysis diagram (Figure 6) was obtained. Mechanical parameters of the soil mass of the model were obtained by direct shear test (Table 2).

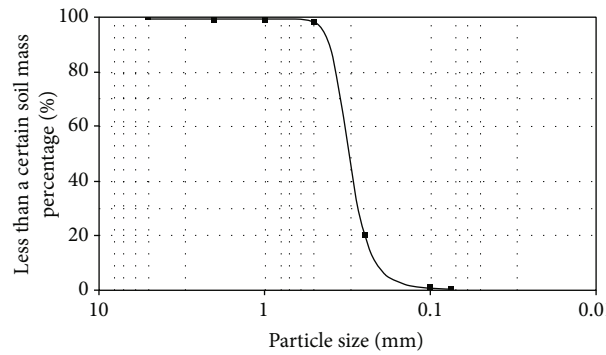

Figure 6: Grain analysis diagram of soil.

The thickness of the retaining wall locked segment of the landslide model is 1 cm. It was made by complete mixing of gypsum, fine sand, and water. The ratio of water : gypsum : sand was 1 : 0.8 : 1. The cylindrical sample is made by the ratio, and the sample size is φ50 mm × 100 mm. The uniaxial compressive strength of the cylindrical sample is 1.12 MPa by YAW6206 electrohydraulic servo pressure testing machine (Figure 7).

The bedrock of the model is a combination of gypsum, brick, and mortar, and therefore, it has a high strength and stiffness.

3. Results

According to the earth pressure and loading process curves (Figure 8), the landslide was gradually pushed and squeezed from back to front due to external load, and the earth pressure increased with increasing load. Under the third load, the earth pressure measured by the EPS-2 sensor (812 s) decreased. The reduced earth pressure at this location indicated that the upper part of the landslide lost its stability and shear cracks appeared (Figure 9(a)). The cloud map of the landslide displacement after the third load was obtained by the three-dimensional laser scanning technique. As shown in Figure 10(a), the displacement of the EPS-2 sensor in the upper part was greater than the displacement in the middle part and in the front of the landslide, which further indicated that shear failure occurred in the upper part of the landslide. At the fourth load, the earth pressure at the EPS-3 sensor decreased (1244 s) (see illustration in Figure 8), indicating that the failure occurred in the middle of the landslide.

Table 2: Model soil parameters.

Name	Dry density ρ_d (g/cm^3)	Moisture content ω (%)	Cohesion c (kPa)	Internal friction angle (°)
Model test soil	1.68	9	0.5	36.2

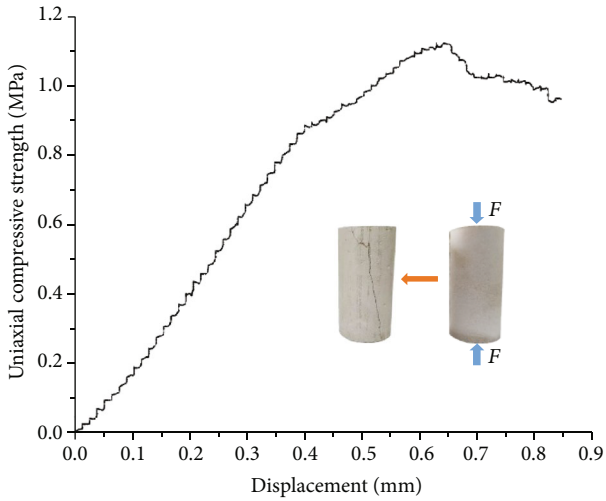

Figure 7: Uniaxial compressive strength of cylindrical sample with water, gypsum, and sand ratio of 1 : 0.8 : 1.

After the shear failure of the upper part of the landslide, the irresistible load was gradually transferred to the middle and lower parts of the landslide. At the seventh load, the earth pressure decreased at the EPS-4 sensor in the middle of the landslide (2309 s). The reduced earth pressure at this location indicated that the failure range propagates to the middle of the landslide. The sliding mass was gradually pushed and squeezed to the locked segment due to external load, and then part of the surface soil mass in the middle of the locked segment slipped under the influence of the external load. The sliding of the surface soil mass on the locked segment caused a slight decrease in the earth pressure at the EPS-5 sensor location (2675 s), and the retaining wall locked segment was exposed to the surface (Figure 9(b)). According to the cloud map of the landslide displacement under seventh load (Figure 10(b)), the displacement of the middle part of the landslide further increased under the external load, while the displacement of the retaining wall locked segment decreased due to the slipped surface soil mass.

At the tenth load, the landslide was pushed forward under the external load, and the load on the retaining wall locked segment gradually increased. The surface soil mass at the retaining wall was widely exfoliated and slipped, and the retaining wall locked segment was completely exposed to the surface (Figure 9(c)). According to the cloud map of the landslide displacement under the tenth load (Figure 10(c)), the soil mass between the retaining wall and the trailing edge of the landslide was further extruded and uplifted under the external load, so the vertical displacement was further increased to 0.12 m. At the same time, the surface soil mass on the retaining wall locked segment slipped in a wide range due to pushing and squeezing, which resulted in a decrease in the value of vertical displacement (Figure 10(c)).

According to the earth pressure and loading process curves (Figure 8), the earth pressure at the landslide sensors decreased sharply at the tenth load time (3572 s). By analyzing the slope shape (Figure 9) and high-definition photos of the side of the landslide (Figure 11), it can be noticed that the landslide was pushed and squeezed to the retaining wall locked segment under external load, and the load of the sliding mass was transferred to the retaining wall. The locking effect of the retaining wall caused the soil to extrude and uplift at the trailing edge of the retaining wall. The load continued to increase and exceeded the shear strength of the soil at the trailing edge of the retaining wall, and the landslide formed a shallow sliding surface that resulted in shallow instability and failure. Due to the shallow landslide failure, the earth pressure dropped sharply. As the load continued to increase, the sliding mass continued to push and squeeze under the load, and the earth pressure curves increased again. Then, the part of the sliding mass above the shallow sliding surface collapsed (Figure 9(c)), and the earth pressure curves decreased again (3727 s).

As the model continued to be loaded for the eleventh time, the soil mass at the trailing edge of the locked segment pushed and squeezed the retaining wall, resulting in compression-shear fracture failure (Figure 12). The total landslide failure was caused by the failure of the locked segment (Figure 9(d)), and the earth pressure decreased sharply at each sensor (4031 s).

In order to further analyze the deformation process of the landslide with retaining wall locked segment under external load, the deep displacement monitoring points on the landslide side (from DMP-1 to DMP-4) were used (Figure 5). DMP-1 and DMP-2 were located in the upper and middle part of the landslide, respectively, while DMP-3 and DMP-4 were placed on both sides of the retaining wall locked segment. According to the displacement curves of the monitoring points (Figure 13), displacement of DMP-1 and DMP-2 increased with the increase of load during the initial stage of loading and then entered the stable deformation phase. The displacement of the monitoring points was small before the compression-shear fracture of the retaining wall locked segment. The overall landslide failure, caused by the failure of the locked segment, led to the sharp increase in the displacement of the monitoring points (Figure 13(a)). The displacement of DMP-3 and DMP-4 changed slightly with the load, while it increased sharply after the overall landslide failure caused by the compression-shear fracture of the retaining wall locked segment (Figure 13(b)). The analysis of the evolution process of deep displacement and deformation can further validate the controlling effects of the retaining wall locked segment on the landslide stability.

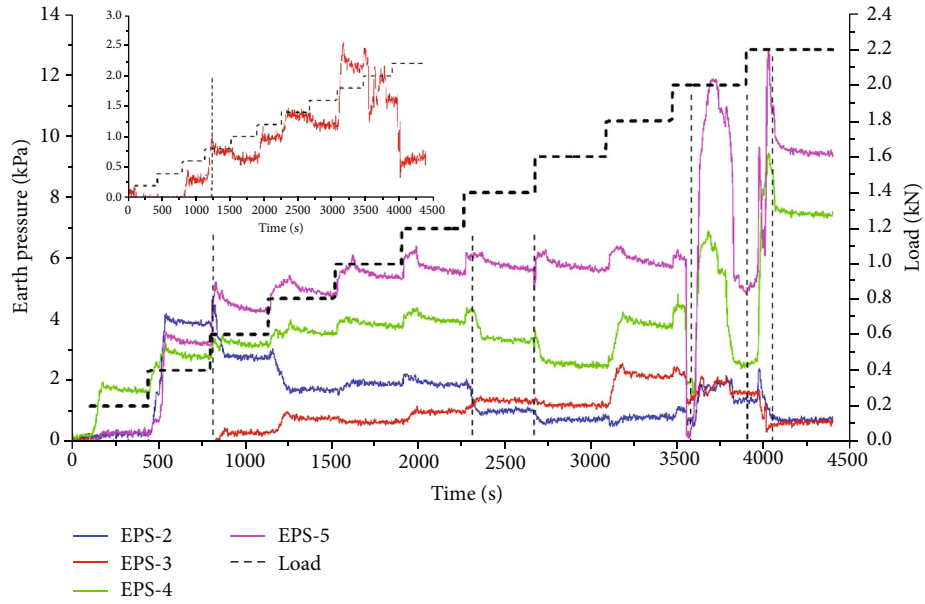

Figure 8: Curves of earth pressure and load.

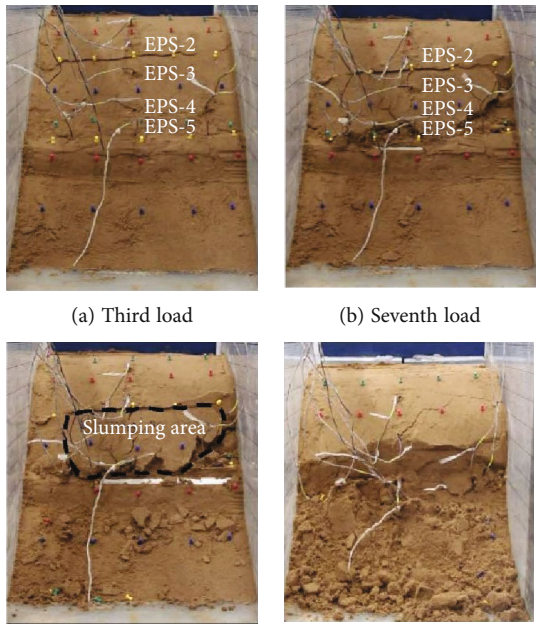

(a) Third load (b) Seventh load

(c) Tenth load (d) Eleventh load

Figure 9: Evolution of landslide with retaining wall locked segment.

4. Discussion

Understanding the failure mechanism of the locked segment type landslide is of great importance for accurate prediction of landslide failure [2]. At present, a great deal of research has been carried out on the classification and instability prediction theory of the locked segment type landslide [1, 2, 19, 26, 28, 31–33].

For landslide with retaining wall locked segment, Chen et al. [2] classified the locked segment type landslide and generalized the geological model of the landslide with retaining wall locked segment, but did not carry out experimental research. Huang [19] analyzed the instability mode of typical landslide with retaining wall locked segment, but did not study the entire evolution process of landslide with retaining wall locked segment from incubation, development to failure. Chen et al. [26] performed small-scale direct shear tests of a rock bridge locked segment and indicated that this segment had typical brittle failure characteristics, but no large-scale physical model test was carried out. Liu et al. [51]

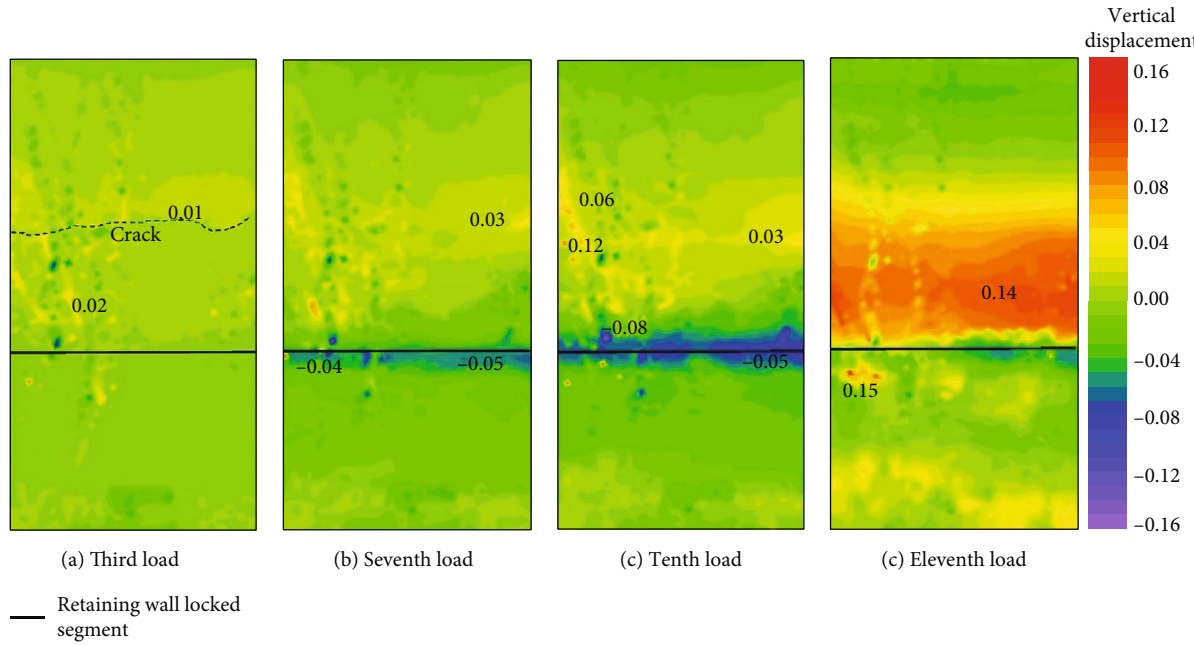

Figure 10: Cloud maps of the cumulative vertical displacement of the landslide with retaining wall locked segment.

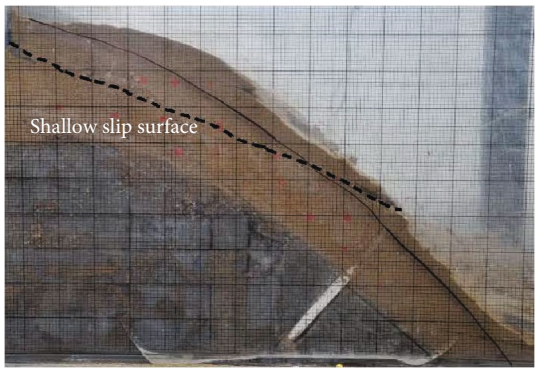

Figure 11: Shallow slip surface of the landslide.

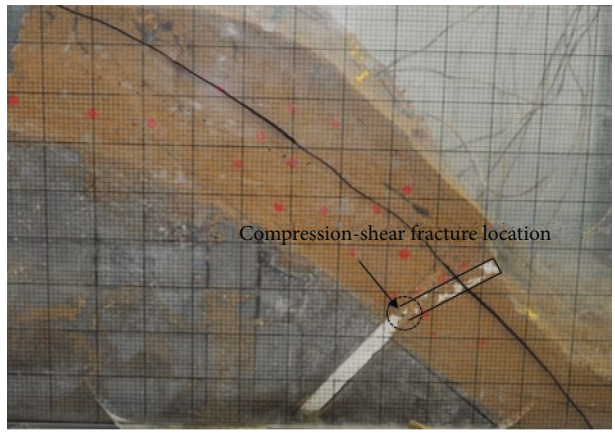

Figure 12: Fracture of the retaining wall locked segment.

carried out the physical model tests to study the catastrophe process and macroscopic deformation instability characteristics of the landslide with retaining wall locked segment under rainfall conditions. However, there are few studies on the evolution mechanism of landslide with retaining wall locked segment under external load by physical model test.

Physical model test is an important method to study the mechanism of landslide evolution. This paper carried out the physical model test of the evolution mechanism on the landslide with retaining wall locked segment. Based on a combination of sensing elements, the stress response and deformation characteristics in the evolution process of the landslide with retaining wall locked segment are analyzed, and the evolutionary instability process and failure mechanism are discussed. The instability process of the landslide with retaining wall locked segment can be summarized as follows. Under external loads such as earthquake and rainfall, the trailing edge of the landslide with retaining wall locked segment is compacted and compressed and then gradually pushed forward and squeezed. Shear failure and shear cracks appear successively at the upper and middle parts of the landslide. After the failure of the upper and middle parts, the sliding mass is gradually pushed and squeezed to the locked segment due to external loads. Then, the sliding mass transfers the irresistible load to the retaining wall. The locking effect causes the sliding mass at the trailing edge of the retaining wall to be squeezed and raised. With increasing load, shallow slip surface forms and the sliding mass at the trailing edge of the locked segment pushes and squeezes the retaining wall, which results in the compression-shear fracture failure. Failure of the locked segment leads to the overall failure of the landslide. Based on the evolutionary instability process of the landslide with retaining wall locked segment, the failure mechanism is revealed.

At present, there are few monitoring methods for deep displacement in physical model test. The deep displacement

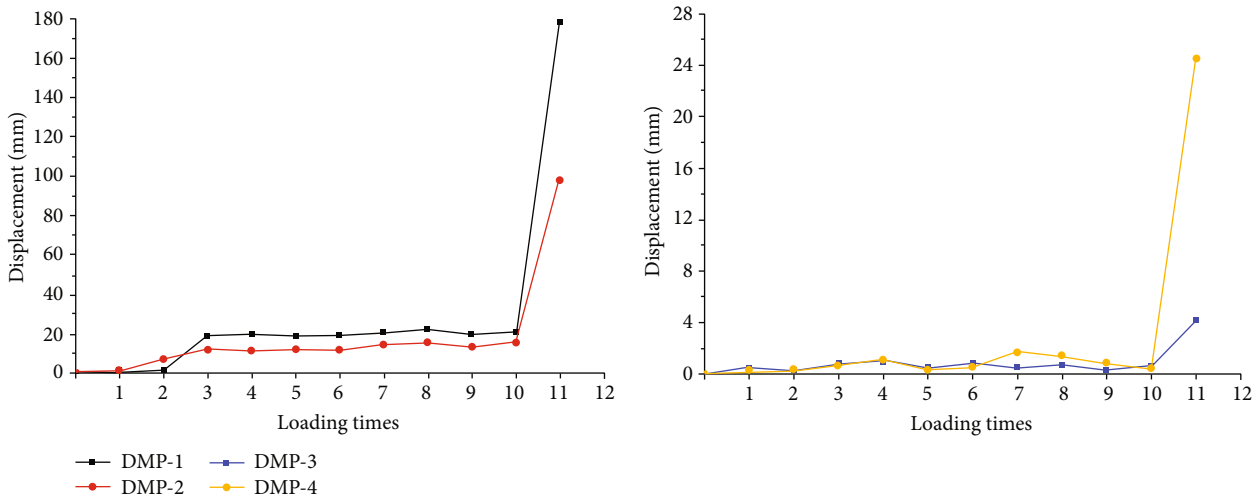

(a) DMP-1 and DMP-2

(b) DMP-3 and DMP-4

Figure 13: Monitoring points displacement curves with loading times.

monitoring points on the landslide side were used in the model test (Figure 5) and achieved good results. Through the deep displacement monitoring results, the locked segment plays an important role in controlling the instability of the locked segment type landslide. Therefore, for the locked segment type landslide engineering case, the displacement of the locked segment, which plays a controlling role in the stability of the landslide, can be monitored. At the same time, according to the proposed evolutionary instability process of the landslide with retaining wall locked segment, the early warning and prediction of landslide are carried out combined with the displacement rate of locked segment.

5. Conclusion

In this paper, the evolution and failure mechanism of the landslide with retaining wall locked segment were analyzed based on physical model test. The main conclusions are as follows:

(1) The results of physical model test of the landslide with retaining wall locked segment show that the retaining wall locked segment represents a sudden brittle failure and plays an important role in the landslide stability control

(2) Based on the deformation and stress response characteristics of the landslide with retaining wall locked segment, its evolutionary instability process is summarized. Under external loads such as earthquake and rainfall, the trailing edge of the landslide with retaining wall locked segment is compacted and compressed, and then gradually pushed forward and squeezed. Shear failure and shear cracks appear successively at the upper and middle parts of the landslide. After the failure of the upper and middle parts, the sliding mass is gradually pushed and squeezed to the locked segment due to external loads. Then, the sliding mass transfers the irresistible load to the retaining wall-locked segment. The locking effect causes the sliding mass at the trailing edge of the retaining wall to be squeezed and raised. With increasing load, the sliding mass at the trailing edge of the locked segment pushes and squeezes the retaining wall, which results in the compression-shear fracture failure. Failure of the locked segment leads to the overall failure of the landslide

(3) The failure mechanism is revealed based on the evolutionary instability process of the landslide with retaining wall locked segment: the upper part of the landslide thrusts and slides; the retaining wall produces a locking effect; the middle part extrudes and uplifts, which is accompanied with shallow sliding; and the compression-shear fracture of the locked segment leads to the landslide failure

Data Availability

The data used to support the findings of this study are included within the article.

Conflicts of Interest

All authors contributed to the study conception and design. No conflict of interest exits in this manuscript, and manuscript is approved by all authors for publication. I would like to declare on behalf of my coauthors that the work described was original research that has not been published previously, and not under consideration for publication elsewhere, in whole or in part.

Authors' Contributions

All authors read and approved the manuscript.

Acknowledgments

This study was supported by the National Key R&D Program of China (no. 2019YFC1509704), the National Natural Science Foundation of China (no. U1704243), and the Doctoral Candidate Innovation Fund of the North China University of Water Resources and Electric Power (B2019081814). The authors especially appreciate the valuable comments of the editors and reviewers that have substantially improved the manuscript.

References

[1] X. U. Lei, Q. I. Siqing, P. A. Xiaohua, C. H. Hongran, Y. A. Baicun, and Z. H. Ke, "Mechanism and physical prediction model of instability of the locked-segment type slopes," *Journal of Engineering Geology*, vol. 26, no. 1, pp. 179–192, 2018.

[2] H. R. Chen, S. Q. Qin, L. Xue, B. Yang, and K. Zhang, "A physical model predicting instability of rock slopes with locked segments along a potential slip surface," *Engineering Geology*, vol. 242, no. 2018, pp. 34–43, 2018.

[3] E. Eberhardt, "Twenty-ninth Canadian geotechnical colloquium: the role of advanced numerical methods and geotechnical field measurements in understanding complex deep-seated rock slope failure mechanisms," *Canadian Geotechnical Journal*, vol. 45, no. 4, pp. 484–510, 2008.

[4] S. Qin, J. J. Jiao, S. Wang, and H. Long, "A nonlinear catastrophe model of instability of planar-slip slope and chaotic dynamical mechanisms of its evolutionary process," *International Journal of Solids and Structures*, vol. 38, no. 44-45, pp. 8093–8109, 2001.

[5] A. Smith, N. Dixon, and G. J. Fowmes, "Early detection of first-time slope failures using acoustic emission measurements: large-scale physical modelling," *Geotechnique*, vol. 67, no. 2, pp. 138–152, 2017.

[6] Y. Zheng, C. X. Chen, T. T. Liu, W. Zhang, and Y. Song, "Slope failure mechanisms in dipping interbedded sandstone and mudstone revealed by model testing and distinct-element analysis," *Bulletin of Engineering Geology and the Environment*, vol. 77, no. 1, pp. 49–68, 2018.

[7] N. Bar, M. Kostadinovski, M. Tucker et al., "Rapid and robust slope failure appraisal using aerial photogrammetry and 3D slope stability models," *International Journal of Mining Science and Technology*, vol. 30, no. 5, pp. 651–658, 2020.

[8] H. Basahel and H. Mitri, "Probabilistic assessment of rock slopes stability using the response surface approach - a case study," *International Journal of Mining Science and Technology*, vol. 29, no. 3, pp. 357–370, 2019.

[9] A. McQuillan, I. Canbulat, and J. Oh, "Methods applied in Australian industry to evaluate coal mine slope stability," *International Journal of Mining Science and Technology*, vol. 30, no. 2, pp. 151–155, 2020.

[10] C. Obregon and H. Mitri, "Probabilistic approach for open pit bench slope stability analysis - a mine case study," *International Journal of Mining Science and Technology*, vol. 29, no. 4, pp. 629–640, 2019.

[11] Z. Tao, Y. Shu, X. Yang, Y. Peng, Q. Chen, and H. Zhang, "Physical model test study on shear strength characteristics of slope sliding surface in Nanfen open-pit mine," *International Journal of Mining Science and Technology*, vol. 30, no. 3, pp. 421–429, 2020.

[12] Y. G. Zhang, X. Q. Chen, R. P. Liao et al., "Research on displacement prediction of step-type landslide under the influence of various environmental factors based on intelligent WCA-ELM in the Three Gorges Reservoir area," *Natural Hazards*, vol. 107, no. 2, pp. 1709–1729, 2021.

[13] Y. G. Zhang, J. Tang, R. P. Liao et al., "Application of an enhanced BP neural network model with water cycle algorithm on landslide prediction," *Stochastic Environmental Research and Risk Assessment*, vol. 35, no. 6, pp. 1273–1291, 2020.

[14] R. Q. Huang, "Large-scale landslides and their sliding mechanisms in China since the 20th century," *Chinese Journal of Rock Mechanics and Engineering*, vol. 26, no. 3, pp. 433–454, 2007.

[15] H. D. Liu, Y. B. Zhang, and L. P. Lu, "Types of the locked section landslide in the western Henan province," *Journal of North China University of Water Resources and Electric Power*, vol. 39, no. 6, pp. 1–7, 2018.

[16] P. A. Xiaohua, X. U. Lei, Q. I. Siqing, L. I. Guoliang, L. I. Pei, and W. A. Miaomiao, "Types, formation conditions and predecision method for large landslides with potential locked patches," *Journal of Engineering Geology*, vol. 22, no. 6, pp. 1159–1167, 2014.

[17] H. M. Tang, Z. X. Zou, C. R. Xiong et al., "An evolution model of large consequent bedding rockslides, with particular reference to the Jiweishan rockslide in Southwest China," *Engineering Geology*, vol. 186, pp. 17–27, 2015.

[18] Y. P. Yin, P. Sun, M. Zhang, and B. Li, "Mechanism on apparent dip sliding of oblique inclined bedding rockslide at Jiweishan, Chongqing, China," *Landslides*, vol. 8, no. 1, pp. 49–65, 2011.

[19] R. Q. Huang, "Mechanisms of large-scale landslides in China," *Bulletin of Engineering Geology and the Environment*, vol. 71, no. 1, pp. 161–170, 2012.

[20] E. Eberhardt, D. Stead, and J. S. Coggan, "Numerical analysis of initiation and progressive failure in natural rock slopes–the 1991 Randa rockslide," *International Journal of Rock Mechanics and Mining Sciences*, vol. 41, no. 1, pp. 69–87, 2004.

[21] H. H. Einstein, D. Veneziano, G. B. Baecher, and K. J. O'Reilly, "The effect of discontinuity persistence on rock slope stability," *International Journal of Rock Mechanics and Mining Sciences and Geomechanics Abstracts*, vol. 20, no. 5, pp. 227–236, 1983.

[22] M. Frayssines and D. Hantz, "Failure mechanisms and triggering factors in calcareous cliffs of the subalpine ranges (French Alps)," *Engineering Geology*, vol. 86, no. 4, pp. 256–270, 2006.

[23] C. Gehle and H. K. Kutter, "Breakage and shear behaviour of intermittent rock joints," *International Journal of Rock Mechanics and Mining Sciences*, vol. 40, no. 5, pp. 687–700, 2003.

[24] J. Kemeny, "The time-dependent reduction of sliding cohesion due to rock bridges along discontinuities: a fracture mechanics approach," *Rock Mechanics and Rock Engineering*, vol. 36, no. 1, pp. 27–38, 2003.

[25] J. Kemeny, "Time-dependent drift degradation due to the progressive failure of rock bridges along discontinuities," *International Journal of Rock Mechanics and Mining Sciences*, vol. 42, no. 1, pp. 35–46, 2005.

[26] G. Q. Chen, Y. Zhang, R. Q. Huang, F. Guo, and G. Zhang, "Failure mechanism of rock bridge based on acoustic emission technique," *Journal of Sensors*, vol. 2015, Article ID 964730, 11 pages, 2015.

[27] R. Q. Huang, G. Q. Chen, and P. Tang, "Precursor information of locking segment landslides based on transient characteristics," *Chinese Journal of Rock Mechanics and Engineering*, vol. 36, no. 3, pp. 521–533, 2017.

[28] S. Q. Qin, Y. Y. Wang, and P. Ma, "Exponential laws of critical displacement evolution for landslides and avalanches," *Chinese Journal of Rock Mechanics and Engineering*, vol. 29, no. 5, pp. 873–880, 2010.

[29] J. Kan, G. Li, N. Zhang, P. Wang, C. Han, and S. Wang, "Study on the fractal characteristics of the pomegranate biotite schist under impact loading," *Geofluids*, vol. 2021, Article ID 6664925, 9 pages, 2021.

[30] Y. Zhou, D. J. Zhao, B. Li, H. Wang, Q. Tang, and Z. Zhang, "Fatigue damage mechanism and deformation behaviour of granite under ultrahigh-frequency cyclic loading conditions," *Rock Mechanics and Rock Engineering*, vol. 54, no. 9, pp. 4723–4739, 2021.

[31] H. R. Chen, S. Q. Qin, L. Xue, B. C. Yang, K. Zhang, and X. W. Wu, "Characterization of brittle failure of rock and limitation of Weibull distribution," *Progress in Geophysics*, vol. 32, no. 5, pp. 2200–2206, 2017.

[32] B. C. Yang, S. Q. Qin, L. Xue, H. R. Chen, X. W. Wu, and K. Zhang, "A physical self-similarity law describing the accelerated failure behavior of rocks," *Chinese Journal of Geophysics*, vol. 60, no. 5, pp. 1746–1760, 2017.

[33] L. Xue, S. Q. Qin, P. Li, G. Li, I. Adewuyi Oyediran, and X. Pan, "New quantitative displacement criteria for slope deformation process: from the onset of the accelerating creep to brittle rupture and final failure," *Engineering Geology*, vol. 182, no. 2014, pp. 79–87, 2014.

[34] H. R. Chen, S. Q. Qin, L. Xue, B. Yang, and K. Zhang, "Modes of mechanical action between locked segments," *Journal of Engineering Geology*, vol. 27, no. 1, pp. 1–13, 2019.

[35] A. Askarinejad, D. Akca, and S. M. Springman, "Precursors of instability in a natural slope due to rainfall: a full-scale experiment," *Landslides*, vol. 15, no. 9, pp. 1745–1759, 2018.

[36] R. A. Beddoe and W. A. Take, "Loss of slope support due to base liquefaction: comparison of 1g and centrifuge landslide flume experiments," *Soils & Foundations*, vol. 56, no. 2, pp. 251–264, 2016.

[37] D. Y. Li, F. S. Miao, Y. H. Xie, and C. Leo, "Hazard prediction for Baishuihe landslide in the three gorges reservoir during the extreme rainfall return period," *KSCE Journal of Civil Engineering*, vol. 23, no. 12, pp. 5021–5031, 2019.

[38] F. Luino, L. Borgatti, and M. Soldati, "Sequence of instability processes triggered by heavy rainfall in the northern Italy," *Geomorphology*, vol. 66, no. 1-4, pp. 13–39, 2005.

[39] J. Ma, X. Li, J. Wang et al., "Experimental study on vibration reduction technology of hole-by-hole presplitting blasting," *Geofluids*, vol. 2021, Article ID 5403969, 2021.

[40] R. Mahalingam and B. Kim, "Factors affecting occurrence of landslides induced by the M7.8 April 2015, Nepal earthquake," *KSCE Journal of Civil Engineering*, vol. 25, no. 1, pp. 78–91, 2021.

[41] V. B. Q. Nguyen and Y. T. Kim, "Rainfall-earthquake-induced landslide hazard prediction by Monte Carlo simulation: a case study of MT. Umyeon in Korea," *KSCE Journal of Civil Engineering*, vol. 24, no. 1, pp. 73–86, 2020.

[42] Q. H. Ran, Y. Y. Hong, W. Li, and J. Gao, "A modelling study of rainfall-induced shallow landslide mechanisms under different rainfall characteristics," *Journal of Hydrology*, vol. 563, no. 2018, pp. 790–801, 2018.

[43] M. Zhang, Y. P. Yin, and B. L. Huang, "Mechanisms of rainfall-induced landslides in gently inclined red beds in the eastern Sichuan Basin, SW China," *Landslides*, vol. 12, no. 5, pp. 973–983, 2015.

[44] Y. G. Zhang, J. Tang, Z. Y. He, J. Tan, and C. Li, "A novel displacement prediction method using gated recurrent unit model with time series analysis in the Erdaohe landslide," *Natural Hazards*, vol. 105, no. 1, pp. 783–813, 2020.

[45] Y. G. Zhang, Z. Zhang, S. Xue, R. Wang, and M. Xiao, "Stability analysis of a typical landslide mass in the Three Gorges Reservoir under varying reservoir water levels," *Environmental Earth Sciences*, vol. 79, no. 1, 2020.

[46] S.-b. Tang, Z. Dong, J.-x. Wang, and A. Mahmood, "A numerical study of fracture initiation under different loads during hydraulic fracturing," *Journal of Central South University*, vol. 27, no. 12, pp. 3875–3887, 2020.

[47] W.-m. Yang, Y. Geng, Z.-q. Zhou et al., "True triaxial hydraulic fracturing test and numerical simulation of limestone," *Journal of Central South University*, vol. 27, no. 10, pp. 3025–3039, 2020.

[48] G. A. Francfort and J. J. Marigo, "Revisiting brittle fracture as an energy minimization problem," *Journal of the Mechanics and Physics of Solids*, vol. 46, no. 8, pp. 1319–1342, 1998.

[49] B. Haimson and C. Fairhurst, "Initiation and extension of hydraulic fractures in rocks," *Society of Petroleum Engineers Journal*, vol. 7, no. 3, pp. 310–318, 1967.

[50] M. Hubbert and D. G. W. Willis, "Mechanics of hydraulic fracturing," *Transactions of the AIME*, vol. 210, no. 1, pp. 153–168, 1957.

[51] H. D. Liu, D. D. Li, Z. F. Wang, Z. Geng, and L. D. Li, "Physical modeling on failure mechanism of locked-segment landslides triggered by heavy precipitation," *Landslides*, vol. 17, no. 2, pp. 459–469, 2020.